

# Tensor interaction constraints from $\beta$ decay recoil spin asymmetry of trapped atoms

J.R.A. Pitcairn,<sup>1</sup> D. Roberge,<sup>1</sup> A. Gorelov,<sup>2</sup> D. Ashery,<sup>3</sup> O. Aviv,<sup>3</sup> J.A. Behr,<sup>4</sup> P.G. Bricault,<sup>4</sup> M. Dombsky,<sup>4</sup> J.D. Holt,<sup>4</sup> K.P. Jackson,<sup>4</sup> B. Lee,<sup>4</sup> M.R. Pearson,<sup>4</sup> A. Gaudin,<sup>4</sup> B. Dej,<sup>4</sup> C. Höhr,<sup>4</sup> G. Gwinner,<sup>5</sup> and D. Melconian<sup>6</sup>

<sup>1</sup>*Department of Physics, University of British Columbia, Vancouver, British Columbia, Canada V6T 1Z1*

<sup>2</sup>*Department of Physics, Simon Fraser University, Burnaby, British Columbia, Canada V5A 1S6*

<sup>3</sup>*School of Physics and Astronomy, Tel Aviv University, 69978 Tel Aviv, Israel*

<sup>4</sup>*TRIUMF, 4004 Wesbrook Mall, Vancouver, British Columbia, Canada V6T 2A3*

<sup>5</sup>*Department of Physics and Astronomy, University of Manitoba, Winnipeg, Canada*

<sup>6</sup>*Department of Physics, Texas A&M University, College Station, Texas, U.S.A.*

We have measured the angular distribution of recoiling daughter nuclei emitted from the Gamow-Teller  $\beta$  decay of spin-polarized  $^{80}\text{Rb}$ . The asymmetry of this distribution vanishes to lowest order in the Standard Model (SM) in pure Gamow-Teller decays, producing an observable very sensitive to new interactions. We measure the non-SM contribution to the asymmetry to be  $A_T = 0.015 \pm 0.029$  (stat)  $\pm 0.019$  (syst), consistent with the SM prediction. We constrain higher-order SM corrections using the measured momentum dependence of the asymmetry, and their remaining uncertainty dominates the systematic error. Future progress in determining the weak magnetism term theoretically or experimentally would reduce the final errors. We describe the resulting constraints on fundamental 4-Fermi tensor interactions.

PACS numbers: 23.40.-s, 32.80.Pj, 14.80.-j

## I. INTRODUCTION

### A. Search for tensor interactions

Effective 4-Fermi contact interactions contributing to beta decay can be classified by the Lorentz transformation properties of the contributing lepton and hadron currents [1]. The Standard Model (SM) of particle physics contains vector (V) and axial vector (A) interactions with sign ‘V-A’. Extensions to the standard model can produce effective scalar and tensor interactions. The observable measured here was developed shortly after the discovery of parity violation by Treiman, who realized its sensitivity to tensor interactions [2].

To lowest order and neglecting the Fermi function, the angular distribution  $W[\theta]$  of the daughter nuclear recoils with respect to the nuclear spin, integrated over all final momenta, is given by [2],

$$W[\theta] = \quad (1)$$

$$\left(1 + \frac{1}{3}cTx_2\right) - x_1(A_\beta + B_\nu)P \cos\theta - x_2cT \cos^2\theta$$

$$P = \frac{\langle M \rangle}{I} \quad (2)$$

$$T = \frac{I(I+1) - 3\langle M^2 \rangle}{I(2I-1)}, \quad (3)$$

with  $I$  the total nuclear spin and  $M$  the spin projection along the quantization axis, so that  $P$  is the vector polarization of the nucleus, and  $T$  is the 2nd-rank tensor alignment. So the recoiling daughter nuclei detected in singles from the  $\beta$  decay of polarized nuclei have spin asymmetry, integrated over all recoil momentum,  $A_{\text{recoil}} = -(A_\beta + B_\nu)$  where  $A_\beta$  and  $B_\nu$  are the  $\beta$  and  $\nu$  asymmetries. The alignment coefficient  $c$  depends on the nuclear

spins and is calculated in Ref. [3] and Section I C.

The coefficients  $x_1$  and  $x_2$  are calculated from integrations over the momentum of the other outgoing particles, and their detailed dependence on the energy release  $Q$  is given in Appendix A. In the limit of high  $Q$ , as is the case for our  $^{80}\text{Rb}$  decay,  $x_1 \xrightarrow{Q \gg m} 5/8$  and  $x_2 \xrightarrow{Q \gg m} 1/2$ . (Note that  $x_1$  vanishes as  $Q \rightarrow 0$ , as it must because the helicity of the  $\beta^+$  vanishes as its momentum decreases to zero.)

For Gamow-Teller decays in the SM,  $A_\beta = -B_\nu$ , so  $A_{\text{recoil}} = 0$  to lowest order. Vector and axial vector currents that couple to right-handed neutrinos also cancel in the sum  $A_\beta + B_\nu$  [4]. That makes  $A_{\text{recoil}}$  sensitive only to fundamental lepton-quark tensor interactions: it is neither sensitive to effective scalars nor to right-handed currents. The exclusive sensitivity to tensor interactions is only true for one other observable, the  $\beta$ - $\nu$  correlation in pure Gamow-Teller decay [5, 6].

The near-zero value of  $A_{\text{recoil}}$  in the allowed approximation for pure Gamow-Teller decays also makes it a very attractive experimental observable; for example, the polarization  $P$  does not have to be known to high precision to extract the new physics. We will see below that recoil-order corrections produce effects  $\sim 0.01$  in the absence of new physics. Note from Appendix A that the recoil spin asymmetry remains proportional to  $A_\beta + B_\nu$  even before the integration over recoil momenta.

#### 1. Explicit sensitivity to 4-Fermi tensor coupling coefficients

The tensor-axial vector Fierz interference term is linear in a particular combination of the 4-Fermi tensor coupling coefficients  $C_T$  and  $C'_T$  [3]:

$$b_T \frac{m}{E_\beta} = \frac{(C_T + C'_T)}{C_A} \frac{m}{E_\beta}. \quad (4)$$

This term appears in the full expression for the decay distribution before integration over the  $\beta$  momentum [3]. It is well-constrained by other experiments in lower-energy  $\beta$  decays [7], so we will cite results below both with it unconstrained and with it constrained to be small. Its inclusion complicates the expressions, so we include it in our full simulations by numerical integration; we also show the full expression (without Fermi function) in Appendix A. Note that Eq. 1 has consciously assumed the Fierz term to be zero [2] to simplify the expressions.

In absence of this Fierz term, the contribution to  $A_{\text{recoil}}$  from non-SM interactions becomes just the product of the 4-Fermi tensor constants  $C_T$  and  $C'_T$  [2]:

$$A_{\text{recoil}} \xrightarrow{b_T=0} A_T = \pm 2\lambda_{I,I'} C_T C'_T / C_A^2 \quad (5)$$

where the  $\pm$  sign is for  $\beta^\pm$  decay. The coefficient  $\lambda_{I,I'}$  is given in Ref. [3] (see Section IC).

The combination  $C_T + C'_T$  describes a tensor interaction that couples to standard model left-handed neutrinos, while the coupling  $C_T - C'_T$  describes an interaction coupling to neutrinos with non-SM helicity [8]. So the sensitivity of  $A_{\text{recoil}}$  to  $C_T C'_T$  produces sensitivity to interactions with both SM and non-SM chirality.

### B. Tensor interactions in other experiments and theory

Until recently, individual nuclear  $\beta$ -decay correlation experiments and global fits have been consistent with the standard model without a tensor interaction [9, 10, 11]. A recent global fit of nuclear and neutron  $\beta$  decay data including scalar and tensor terms coupling only to standard-model left-handed  $\nu$ 's (i.e. assuming  $C_T=C'_T$ ) gives  $C_T/C_A = 0.0086 \pm 0.0031$ , while excluding the latest neutron lifetime measurement [12] from that fit brings the result into agreement with the Standard Model at one standard deviation [8]. Such difficulties in combining many experiments with different systematic errors in global fits can be avoided by dedicated experiments sensitive only to tensor interactions, like the present experiment. So the present measurement becomes useful if it achieves  $\sim 0.01$  accuracy in the recoil asymmetry.

A tensor interaction coupling to right-handed neutrinos would produce a contribution to the mass of the standard model left-handed neutrinos. An order-of-magnitude calculation suggests that if  $|C_T - C'_T|$  were  $\sim 0.02$ , such an interaction would account for neutrino masses  $\sim 3$  eV [13], the present experimental upper limit. This provides a motivation for direct correlation measurements in order to constrain this possible contribution to neutrino masses.

The PIBETA collaboration reported a statistically significant deviation from the standard model [14] in  $\pi \rightarrow \nu e \gamma$  decay that could be explained by a finite tensor interaction. The same group has made further dedicated experiments and now eliminated the possibility of a tensor interaction [15]. The most restrictive limits from  $\pi \rightarrow \nu e \gamma$  decay are on interactions with same chirality as the Standard Model, i.e. constraining a Fierz interference term that is linear in the small tensor term, although the opposite chirality is also considered in Refs. [9, 16]. Sensitivity in the present experiment  $\sim 0.001$  level would be needed to reach the sensitivity probed by the  $\pi$  decay experiments.

A renormalizable tensor interaction can be generated by the exchange of spin-0 leptoquarks [9, 17]. In an example of an explicit model, a recent analysis of the possible one-loop corrections in SUSY models shows they can produce tensor and scalar interactions as large as 0.001 in the Fierz interference term  $b_T$  from left-right sfermion mixing in the first generation, physics that is otherwise difficult to constrain [18].

### C. $^{80}\text{Rb}$ and recoil-order corrections

The decay of  $I^\pi=1^+$   $^{80}\text{Rb}$  is primarily to two states, 74% to the ground  $0^+$  state and 22% to the first excited  $2^+$  state (see Figure 1). The coefficient  $\lambda_{I,I'}$  in Eq. 5 is 1 for the  $1^+ \rightarrow 0^+$  transitions and  $-1/2$  for the  $1^+ \rightarrow 2^+$  transitions. So when averaged over the transitions, the average  $\lambda_{I,I'}$  for  $^{80}\text{Rb}$  is 0.64. The coefficient  $c$  in Eq. 1 is 1 for the  $1^+ \rightarrow 0^+$  transitions, and  $+0.1$  for  $1^+ \rightarrow 2^+$ .

The  $1^+ \rightarrow 0^+$  transition has higher-order corrections in the SM proportional to the weak magnetism form factor  $b_M$  and the induced tensor form factor  $d$  [19]. The contributions to the angular correlation coefficients from these recoil-order terms are scaled by  $E_\beta/M_{\text{nucleon}}$ , and they produce a small nonzero recoil asymmetry within the Standard Model.

These recoil-order terms are given by sums over individual nucleon matrix elements

$$b_M/A = g_M M_{GT} + \langle f | \sum_k \tau_k^+ \vec{l}_k | i \rangle \quad (6)$$

$$d/A = g_A \langle f | \sum_k \tau_k^+ i \vec{\sigma}_k \times \vec{l}_k | i \rangle \quad (7)$$

using the notation of Ref. [20], which has detailed consideration of the recoil-order matrix elements needed here.

The first term in the expression for weak magnetism,  $b_M/A$ , is from the anomalous isovector magnetic moment of the nucleons, and is given by the dimensionless number  $g_M=4.7$  multiplying the Gamow-Teller matrix element  $M_{GT}$ . The second term in  $b_M/A$  requires a detailed nuclear structure calculation with a large fractional uncertainty in this mass region, as deformation effects make shell model calculations difficult. Weak magnetism terms

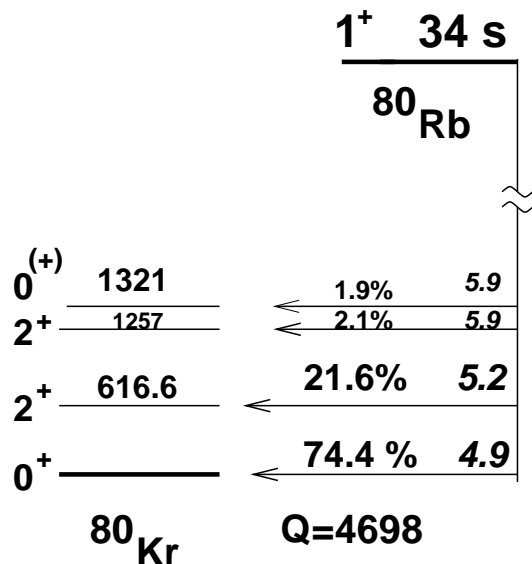


FIG. 1: The  $\beta^+$ -decay scheme for  $^{80}\text{Rb}$ , showing literature values of the spin, parity, branching ratio,  $\log_{10}(ft)$ , and excitation energy of the final levels in  $^{80}\text{Kr}$ , along with the Q-value (maximum kinetic energy) for  $\beta^+$  decay and the parent half-life. Energies in keV.

for a variety of Gamow-Teller decays have been calculated and measured, and the values generally do not depart greatly from the value of  $b_M/(AM_{GT})=4.7$  [19, 20].

The induced tensor term  $d$  is more poorly characterized. We will see below that it contributes values to the experimental recoil asymmetry that are roughly constant with recoil momentum, so we will be able to fit for  $d$  simultaneously with the non-SM tensor interaction.

#### D. Transitions to excited states

The 22%  $1^+$  to  $2^+$  transition in principle adds some complication to the recoil-order matrix elements. The first-order form factors,  $b_M$  and  $d$ , can be different from those for the transition to the ground state. In addition, a total of five additional form factors appear at 2nd-order in recoil terms  $E_\beta/M_{\text{nucleon}}$ . In this version of the experiment, we will let  $b_M$  and  $d$  float phenomenologically below, so that we implicitly include  $b_M$ ,  $d$  for the excited state in our analysis. In other words,  $b_M$  and  $d$  for both the ground and excited states are treated as producing the same functional dependence of the recoil asymmetry on recoil momentum. This is an excellent approximation as the effects on the recoil asymmetry have very similar momentum dependence compared to the ground state, particularly once they are averaged over the momentum spread induced by the final  $\gamma$ -ray emission. The values of  $b_M$  and  $d$  that are extracted are then weighted averages of the transitions. We ignore the 2nd-order terms in  $E_\beta/M_{\text{nucleon}}$ , which is a good approximation at the level of accuracy reached in this version of the experiment.

## II. EXPERIMENTAL TECHNIQUES

We describe below the trap apparatus which we use to polarize the  $^{80}\text{Rb}$  nuclei and measure the angular distribution and momentum of the  $^{80}\text{Kr}$  daughter.

The collection and trapping of the  $^{80}\text{Rb}$  used a two-trap apparatus [21] very similar to that in previous  $\beta$ -decay work [22, 23]. The  $^{80}\text{Rb}$  30 keV ion beam from the ISAC facility at TRIUMF was  $\approx 2 \times 10^9/\text{sec}$  from a zirconium carbide target. The ion beam was stopped in a neutralizing foil made of zirconium. The resulting atoms were collected in the first magneto-optical trap (MOT) [24]. The trapped atoms were transferred to the second MOT to minimize backgrounds [21] and provide an environment for polarization. The number of atoms continuously trapped in the detection trap was  $\approx 2 \times 10^6$ .

### A. Detection geometry

The detection geometry is shown in Fig. 2. The time-of-flight (TOF) of the daughter nuclei from nuclear  $\beta$  decay in singles (i.e. not in coincidence with the  $\beta$ ) can be measured by using the atomic shakeoff electrons as a trigger, as developed by LBL researchers [25]. A uniform electric field of average value 800 V/cm collects ions produced in  $\beta$  decay to a 25 mm diameter microchannel plate (MCP) Z-stack for time readout, backed by a position-sensitive resistive anode. The electric field also collects the atomic electrons to a second MCP detector on the opposite side. A positive ion produced in  $\beta^+$  decay will ‘shake off’ at least two atomic electrons, and electrons up to  $\sim 100$  eV energy are completely collected by the field into the detector. So this technique increases the efficiency for recoil detection by a factor of about 30 compared to  $\beta^+$  detection (which had solid angle 1% in our geometry [22]). This produced approximately 100 Hz of daughter recoils in coincidence with the electron detector, for the average number of atoms trapped of about  $2 \times 10^6$ .

The electron detection geometry and electric fields are optimized to ensure efficient detection independent of the electron’s initial kinetic energy and angle. We measured  $\approx 35\%$  detection efficiency for low-energy electrons from the laser photoionization of  $^{80}\text{Rb}$  (Fig. 3). By photoionizing stable  $^{85}\text{Rb}$ , we have reproduced data in the literature showing that the electron efficiency of MCPs is optimized at 500 eV impact energy, and changes by less than 10% between 500 and 1000 eV [28]. The shakeoff electrons are expected to have kinetic energies similar to their atomic binding energies, a few 10’s of eV [29], so we arrange the fields so that the electrons impact the MCP with approximately 500 eV more than their original kinetic energy. To make the electric field more uniform in the region traversed by the electrons than in the geometry of Ref. [22], the grid in front of the electron detector is biased to a potential close to that of the final electrode

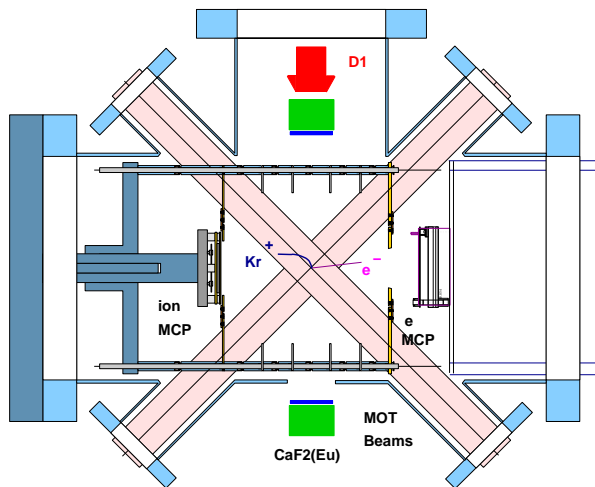


FIG. 2: (Color online) TRINAT detection apparatus. The MCP for ion detection has position-sensitive resistive anode readout. Given the known uniform electric field, measurement of the recoil ion TOF and impact position determines the initial momentum. The apparatus is similar to that of [22], with an MCP for electron detection added for the  $^{80}\text{Rb}$  decay asymmetry. The  $^{80}\text{Rb}$  is spin-polarized by optical pumping with light resonant to the D1 transition from a 50 mW diode laser. The polarization is monitored with  $\beta$   $\Delta E - E$  phoswiches using plastic/ $\text{CaF}_2(\text{Eu})$  fast/slow scintillators (which are at  $-30$  and  $150$  degrees out of the plane shown here).

in the field assembly.

### B. Polarization techniques

The  $^{80}\text{Rb}$  atoms are polarized by switching off the MOT light and optically pumping with light at the D1 transition (see Fig. 3) for  $30 \mu\text{s}$ . Then the MOT light is switched on again for  $30 \mu\text{s}$  to keep the atom cloud from expanding. The MOT 3 G/cm (horizontal) quadrupole field stays on at all times. In a typical MOT with beams carefully balanced in power, the atom cloud would be centered at zero magnetic field, but such a cloud would sample nonzero fields and the polarization would be disturbed by Larmor precession. In order to add a constant magnetic field along the optical pumping axis, we attenuate two of the beams in the MOT horizontal plane, perpendicular to the quadrupole field anti-Helmholtz coil axis. The cloud equilibrium position is then at finite B field, i.e. at a location where Zeeman shifts produce equal absorption from the unbalanced beams. Then we in addition apply at all times a uniform field constant of 2.5 G with Helmholtz coils. The result is a cloud equilibrium position at the center of the apparatus, with on average a 2.5 G field along the optical pumping axis. The cloud spatial FWHM of 3 mm samples  $\pm 0.5$  Gauss of changing field.

Atoms were transferred from the 1st trap every 1.5

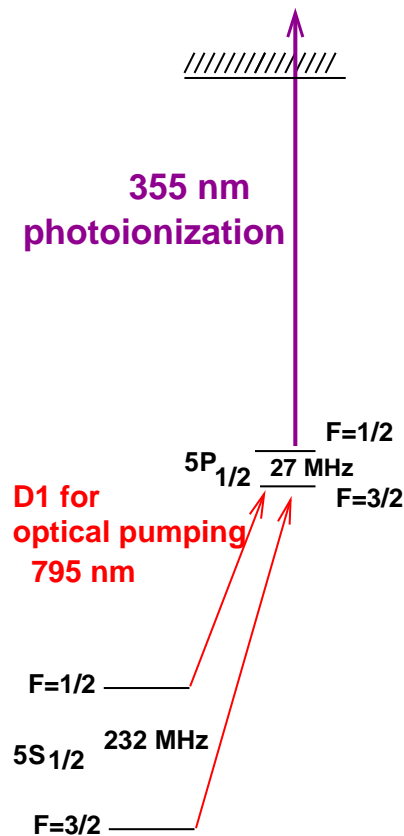


FIG. 3: (Color online) Energy diagram of the atomic levels for optical pumping of the Rb atom, along with the photoionization scheme for position determination. The atomic hyperfine structure is not to scale. The frequency splittings were taken from [27].

seconds. After each transfer, the polarization state was flipped by changing the handedness of the optical pumping light with a liquid crystal variable retarder.

The  $30 \mu\text{s}$  trap on/off polarization off/on duty cycle was chosen to minimize the motion of the cloud during the optical pumping time, which was a dominant systematic in  $\nu$  asymmetry measurements in  $^{37}\text{K}$  [23]. The 2.5 G bias B field means that there were slightly different Zeeman shifts for the two different polarizations. To minimize differences in the atom cloud position, the optical pumping laser frequency was shifted (by less than a linewidth) between the two polarizations.

The atom cloud position was monitored by photoionizing a small fraction of the atoms with a pulsed laser (see Fig. 3) and recording MCP position and TOF. The average trap location was found to shift by  $0.030 \pm 0.003$  mm with spin flip, which would produce a false asymmetry  $A_{\text{recoil}}$  of  $0.0012 \pm 0.0001$ . The correction was made to the data by using the measured trap location when determining the experimental angle of emission below (Section III).

### C. TOF spectrum

We show a typical TOF spectrum in Fig. 4, deconstructed into its components. The different charge states are separated in TOF by a uniform 0.8 kV/cm electric field. Charge states 1, 2 and most of charge state 3 are relatively clean of background. Ions from the 1.4% electron capture branch have a large spin asymmetry and contaminate the higher charge states, and because their asymmetry is large they become a useful probe of the polarization (see below). Note that only about 15% of the  $\beta^+$  decays produce positive ions, as opposed to most of the electron capture decays.

We measured the background from  $\beta^+$ 's striking the electron detector by lowering the bias voltage of the detector to exclude the atomic electrons, while keeping the grid in front of the detector at the same voltage to keep the electric field for ion collection the same. That background has the expected large spin asymmetry from  $\beta$ -recoil coincidences, which in this geometry is determined by the  $\nu$  asymmetry [23]. The recoil asymmetries shown below have been corrected for this background, which produces 1.2% of the charge state 1 recoils, 0.59% of the charge state 2 recoils, and 0.51% of the charge state 3 recoils. The average asymmetry correction can be seen below in Section III, Fig. 9 and will be discussed there.

There is in addition a 1% background between 1.2 and 1.4  $\mu\text{s}$  that shows a definite localization on the lower part of the ion MCP. This background also appears in natural backgrounds and  $\gamma$ -ray source measurements, and may be due to an electronic artifact. Although its origin is not fully understood, we have measured its spin asymmetry to be negligibly small and consistent with zero, so via this technique we can correct for its presence to sufficient accuracy.

### D. Vector polarization determination

Here we describe the determination of the nuclear vector polarization achieved,  $0.55 \pm 0.04$ . The precision is more than adequate because the present observable vanishes, though the final error on the new physics parameters  $A_T$  and  $b_T$  is compromised because it scales inversely with the absolute polarization achieved.

The polarization was optimized by measuring the time dependence of the atomic excited state population during the optical pumping, monitored by non-resonant photoionization with a small pulsed laser (Fig. 3). The excited state population decreases as the polarization increases: if the atoms become fully polarized, then the atom can absorb no more light in this transition and the excited state population would vanish. Equilibrium polarization is reached during the last 20  $\mu\text{s}$  of the optical pumping, during which  $A_{\text{recoil}}$  is measured. Unlike in our previous work with the MOT magnetic quadrupole field turned off [23], we found that the atomic measurement of the polarization was difficult to quantify with the

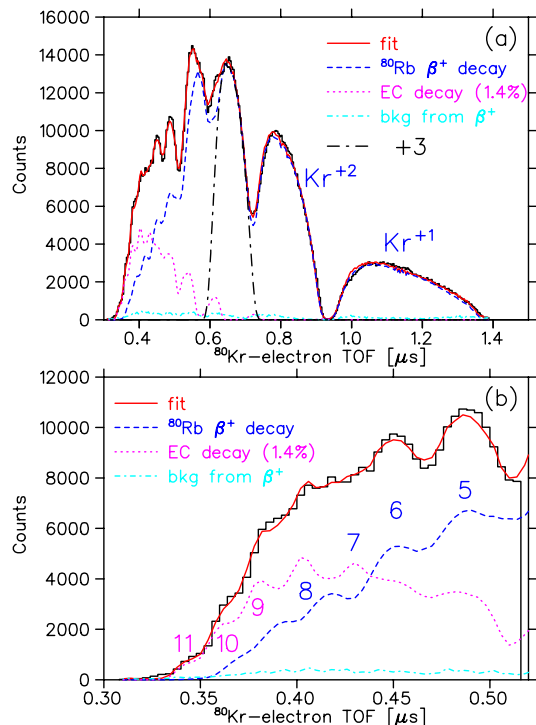


FIG. 4: (Color online) (a) Time-of-flight (TOF) spectra for recoil coincidences with shakeoff atomic electrons, showing decomposition into  $\beta^+$  decay and backgrounds. The small electron capture (EC) branch produces large corrections for the higher charge states, and is modelled here assuming charge state distributions from x-ray photoionization [26]. A background of order 1% from  $\beta^+$ 's striking the electron detector is determined by biasing the detector to exclude low-energy electrons (see text). The simulation for charge state +3 is highlighted; the TOF for +3 was cut above 0.63  $\mu\text{s}$  to help exclude EC events. (b) Expanded TOF scale of the top figure, showing the charge states 9, 10, and 11 that are dominated by EC and used for polarization determination (Section II D).

MOT quadrupole field left on. So the polarization was measured by nuclear observables.

The  $\beta^+$  asymmetry was measured using plastic/ $\text{CaF}_2(\text{Eu})$  phoswich detectors, in coincidence with shakeoff electrons to minimize sensitivity to decays from untrapped atoms. The phoswiches are located at  $-30$  and  $150$  degrees with respect to the polarization direction, out of the plane of Fig. 2.

The  $\beta$  asymmetry for the  $1^+$  to  $0^+$  transition is  $+1$ , while for the  $1^+$  to  $2^+$  it is  $-1/2$ . So the asymmetry grows at the higher  $\beta$  energies, as the contribution of the  $1^+$  to  $2^+$  becomes proportionately smaller. Figure 5 shows the fit asymmetry as a function of  $\beta$  momentum. For betas in coincidence with recoils in charge states  $+4$  to  $+9$ , the full solid angle of the recoils is detected, so this physical observable is the same as the singles  $\beta$  spin asymmetry. It has the advantage of being completely clean of background from decaying atoms that are not in the trap. The result is  $P=0.53 \pm 0.03$ .

An entirely different nuclear observable serves as an

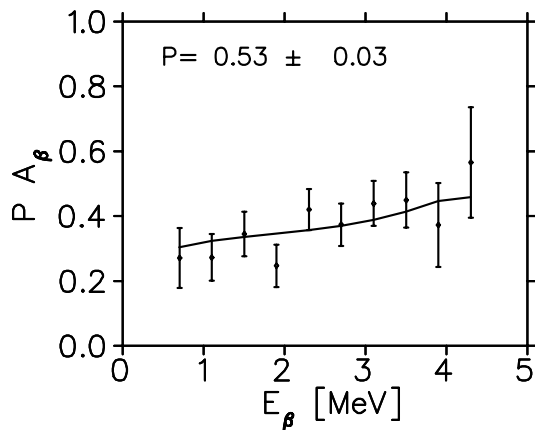


FIG. 5: Nuclear polarization determined from the  $\beta$  asymmetry in coincidence with Kr recoils charge states 4-9 in the CaF<sub>2</sub>(Eu) detectors.

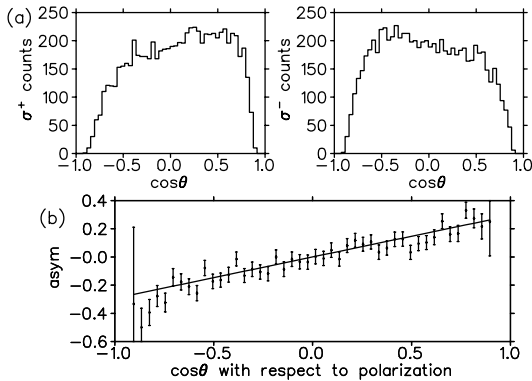


FIG. 6: Nuclear polarization determined from recoils from electron capture (EC) decay (see text), which has a large spin asymmetry. (a) Counts as a function of  $\cos \theta$  for opposite signs of polarization. (b) The resulting asymmetry of events from (a); the line is a fit with  $PA_{EC}=0.29\pm 0.02$  (see text).

additional measurement of the nuclear polarization. Recoils produced in electron capture (EC) decay dominate the higher charge states 9, 10, and 11 (see Figure 4(b).) A further cut on recoil momentum removes a 25% contribution from  $\beta^+$ -produced recoils, leaving a clean sample of the highest-momentum EC-produced recoils. Figure 6(b) shows the angle dependence (as constructed from the MCP position information and time-of-flight) of the resulting recoils from EC. If the polarization  $P$  were unity, the EC recoils would have asymmetry unity for the  $1^+$  to  $0^+$  transition, and -0.5 for the  $1^+$  to  $2^+$  transition. A simple linear fit to the asymmetry in Figure 6(b) (there is no  $\cos^2\theta$  term [2]), extracts  $PA_{EC}=0.29\pm 0.02$ , which implies nuclear polarization  $P=0.57\pm 0.04$ .

In summary, the nuclear vector polarization achieved from these consistent observables is  $0.55 \pm 0.04$ . The uncertainty produces an error on the extracted  $A_{\text{recoil}}$  of 7% of its value, which as we will see below is negligibly small in this version of the experiment.

## E. Tensor alignment

We have no direct observables that are very sensitive to the tensor-order polarization alignment  $T$  (defined in Eq. 3), but we can make adequate indirect constraints from the measured vector polarization  $P=0.55\pm 0.04$ . For nuclear spin  $I=1$  and  $P<1$ , the population that is not in spin projection  $m_I=1$  must obviously either be in  $m_I=0$  or  $-1$ . If it were all in  $m_I=-1$ , then the value of  $T=-1$ , unchanged from its value for perfect  $P=1$ . For imperfect optical pumping spoiled by Larmor precession in the quadrupole field, it is much more likely for most of the population to be in  $m_I=0$ ; doing this produces our best estimate of  $T=0.35$ . In the fits, these two extremes do not significantly perturb the extracted asymmetry coefficients  $A_1$ , so we do not mention them further, and simply take  $T=0.35$  in the remaining analysis.

## III. ANALYSIS OF RECOIL ASYMMETRY AS A FUNCTION OF RECOIL MOMENTUM TO EXTRACT RECOIL-ORDER TERMS

From the ion MCP hit position, ion TOF, trap cloud location from photoionization, known uniform electric field, and known charge states 1-3 from range of TOF, we can construct the momentum of the recoil and its emission angle with respect to the polarization direction. By fitting the angular distribution of the recoils for different momentum bins, we can extract the recoil asymmetry as a function of recoil momentum.

The dependence on recoil momentum allows us to extract information about the recoil terms while simultaneously fitting for the tensor interaction. These different terms produce a different functional dependence of the recoil asymmetry on momentum.

If we were to integrate over all momenta, the measured asymmetry  $A_{\text{spin}}$  as the spin polarization  $P$  is flipped can then be found from Eq. 1:

$$\begin{aligned} A_{\text{spin}} &= \frac{W[\theta, P] - W[\theta, -P]}{W[\theta, P] + W[\theta, -P]} \\ &= \frac{x_1 P A_{\text{recoil}} \cos\theta}{1 + cT x_2 + cT x_2 \cos^2\theta} \end{aligned} \quad (8)$$

still ignoring recoil-order terms. An example of such a fit that could extract the quantity  $PA_{\text{recoil}}$  is shown in Fig. 7.

We wish to generalize this to a fit of the recoil asymmetry as a function of recoil momentum. In the absence of the Fermi function and of recoil-order corrections, we could define the recoil asymmetry as a function of recoil momentum  $A_{\text{spin}}[P_r]$  in terms of the kinematic functions of Appendix A:

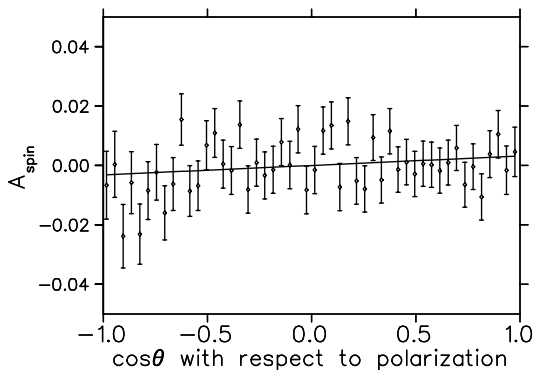


FIG. 7: An example of the recoil asymmetry fit as a function of angle, with angle reconstructed from the impact location and the ion TOF. Here the asymmetry is for the charge state 2 data, summed over all recoil momentum.

$$A_{\text{spin}}[P_r] = \frac{W[\theta, P, P_r] - W[\theta, -P, P_r]}{W[\theta, P, P_r] + W[\theta, -P, P_r]} = \quad (9)$$

$$\frac{(f_4 A_T - f_7 b_T) P \cos \theta}{f_1 - b_T f_6 - (a_{\beta\nu} + \frac{cT}{3}) f_2 + cT(f_3 + f_5 \cos^2(\theta))}$$

where all the  $f_i$  functions depend on  $P_r$ . However, we must properly include the Fermi function (which does not matter quantitatively) and the recoil order terms (which do matter). So instead we write the simple expression actually used for the fits as a function of angle, for each bin of recoil momentum:

$$A_{\text{spin}}[P_r] = \frac{P A_1[P_r] \cos \theta}{1 + cT F_2[P_r] \cos^2 \theta} \quad (10)$$

where  $F_2[P_r]$  now contains all the numerical integrations needed for the  $\cos^2(\theta)$  terms. These fits let us extract the experimental coefficient of  $\cos(\theta)$  of the recoil asymmetry,  $A_1[P_r]$ . We then will fit  $A_1[P_r]$  below, using the different dependence on recoil momentum of the new tensor physics terms and the recoil order terms, in order to extract the tensor physics terms  $A_T$  and  $b_T$ .

We show one experimental example of the spin-flip asymmetry  $A_{\text{spin}}[\theta]$  as a function of  $\cos(\theta)$  in Fig. 7. We make similar fits to  $A_{\text{spin}}$  as a function of binned recoil momentum from 0.5 to 5.0 MeV/c to extract  $A_1[P_r]$ .

#### A. Experimental results for $A_1[P_r]$

We show the results for  $A_1[P_r]$  broken down for the different charge states in Figure 8. The first three charge states can be seen to be statistically consistent. We therefore simply take the weighted average over the charge states to consider the physics below.

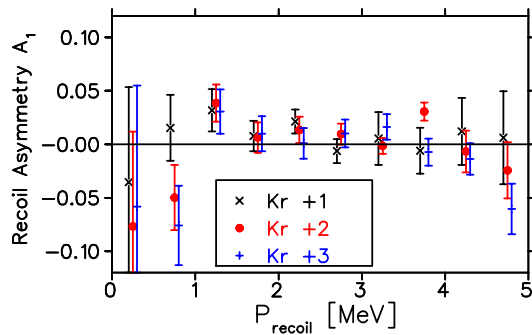


FIG. 8: (Color online) The dependence on recoil momentum of the experimental recoil asymmetries  $A_1$ . Charge states 1, 2, and 3 are shown to be in statistical agreement. (The points for charge states 1 and 3 are offset horizontally for clarity.)

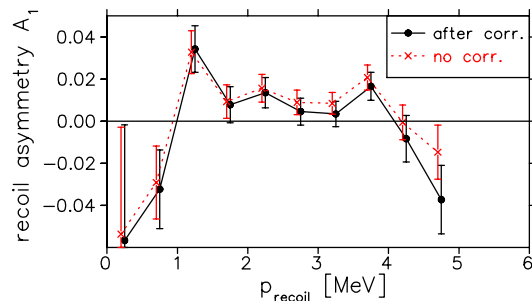


FIG. 9: (Color online)  $A_1$  as a function of recoil momentum, determined with no correction for  $\beta$ 's and after the correction for  $\beta^+$ 's described in Section II C. The correction is small. Lines are drawn only to direct the eye.

#### B. Correction for $\beta^+$ 's striking MCP

Since there is generally concern in precision  $\beta$  asymmetry experiments with the size of any corrections, we show in Figure 9 the results for  $A_1$  with and without the correction from  $\beta^+$ 's striking the electron MCP, as described in Section II C. The final answer for the average  $A_{\text{recoil}}$ , shown below, becomes more negative by about 0.01 when the  $\beta^+$  correction is made. We know this correction to better than 5% of its value.

### IV. RESULTS OF FITS TO THE EXPERIMENTAL $A_1$

We now show results for fits to the extracted average  $A_1[P_r]$ . We try to take advantage of the different momentum dependence produced by the recoil-order corrections  $b_M$  and  $d$ , and the non-SM tensor physics parameters  $A_T$  and  $b_T$ . We consider different constraints on the parameters, partly in hopes that in the future values of the recoil-order corrections may be available.



### A. All parameters floating

First we let all parameters float. We consider various points in the  $C_T + C'_T$  vs.  $C_T - C'_T$  plane, let  $b_M$  and  $d$  float for each point, and compute the  $\chi^2$ . We show the 90% CL limits in a contour plot in Fig. 10, including constraints from other experiments. The best fit is for  $b_M/(AM_{GT})=-7.2\pm 5.0$ , a negative value with rather large absolute value, and a small value of  $d/A=0\pm 17$ . The square root of the reduced  $\chi^2/N$  is 1.37 for the best fit, so we expanded the error bars on the fit parameters accordingly.

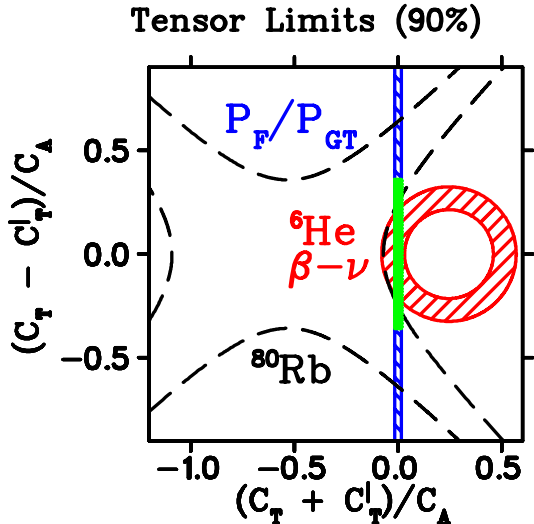


FIG. 10: (Color) Exclusion plot at 90% confidence showing complementarity of the present constraints to other measurements. Allowed regions are inside:  ${}^6\text{He } \beta\text{-}\nu$  [5, 6], red concentric circles (hashed in between);  $\beta^+$  polarization in  ${}^{14}\text{O}$ ,  ${}^{10}\text{C}$  [7] (assuming no scalar interaction), blue solid vertical lines (hashed in between); Present work, letting  $b_M$ ,  $d$ , and both  $A_T$  and  $b_T$  float, black dashed hyperbolae. For  $b_T$  set to 0 (consistent with [7]), weak magnetism  $b_M/(AM_{GT})=4.7 \pm 4.7$ , and  $d$  left floating, then the green rectangular area indicates the present limit  $|(C_T - C'_T)/C_A| < 0.36$ .

As a tool to discuss this result, we show the individual contributions from  $b_M$ ,  $d$ ,  $A_T$ , and  $b_T$  in Fig. 11. The momentum dependence of  $A_1$  from the non-SM tensor terms  $A_T$  and  $b_T$  is similar, so they are both made large with opposite signs to fit the data. The asymmetries produced by these non-SM tensor terms in this fit are therefore much larger in absolute magnitude than the experimental asymmetries.

So a completely unconstrained fit does not produce competitive limits in a model with all chiralities of tensors possible and no constraints on the recoil order terms, because of the large number of similar degrees of freedom. It is also clear that the statistical precision of the data would be much better than the size of these error bars, if other constraints on the physics were applied.

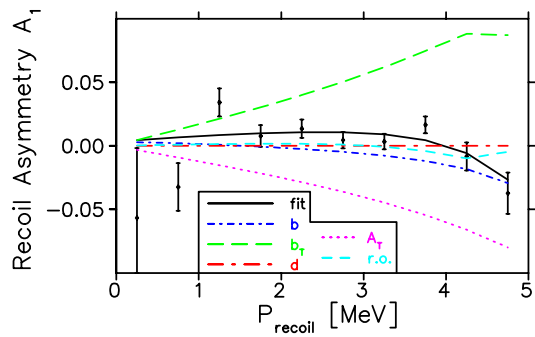


FIG. 11: (Color online) The dependence on recoil momentum of the recoil asymmetries for the best fit with  $b_M$ ,  $d$  and both chiralities of tensor floating.  $\sqrt{\chi^2/N}=1.37$  for this fit. The cyan medium-dash line ‘r.o.’ is a small exact recoil-order correction given when recoil energy is included in the energy conservation equation.

### B. Constraining $C_T + C'_T=0$

We next use the relative positron polarimetry experiments comparing pure Fermi  ${}^{14}\text{O}$  and the pure Gamow-Teller  ${}^{10}\text{C}$  branch [7] to imply that the Fierz interference term  $b_T \propto C_T + C'_T$  is very small. We continue to let  $b_M$ ,  $d$ , and  $A_T$  float.

The resulting constraints on  $C_T - C'_T$  can simply be seen by looking at the intersection of our limit hyperbolae with the the  $C_T + C'_T=0$  axis of Fig. 10. A more detailed look at the  $\chi^2$  minimum implies  $|(C_T - C'_T)/C_A|=0.42^{+0.15}_{-0.32}$  at 90% confidence, and the resulting recoil order terms are  $b_M/(AM_{GT})=-18\pm 11$  and  $d/A=24\pm 41$ . Note here that  $b_M$  lies far outside the nucleon value.

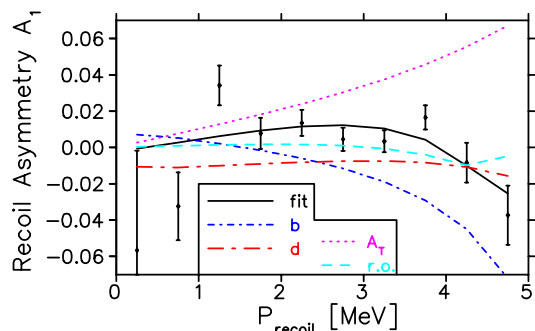


FIG. 12: (Color online) The dependence on recoil momentum of the recoil asymmetries for the best fit with  $C_T + C'_T=0$  (i.e. assuming the result of Ref. [7]), and  $b_M$ ,  $d$  and  $C_T - C'_T$  floating. The fit has  $\sqrt{\chi^2/N}=1.41$ , and the result is  $|(C_T - C'_T)/C_A| = 0.42^{+0.15}_{-0.32}$  at 90% confidence.

The breakdown into the various contributions is shown in Fig. 12. Here it can be seen that  $b_M$  and  $A_T$  produce contributions to  $A_1$  with similar momentum dependence, so again it is difficult to fit them both simultaneously. It also is clear the the contribution to  $A_1$  from  $d$  is comparatively constant with momentum, so  $d$  can be floated in



a meaningful fashion.

### C. Constraining $C_T + C'_T=0$ and constraining $b_M$ from theory

Here we keep  $C_T + C'_T=0$  from the literature, and also constrain the weak magnetism term  $b_M/(AM_{GT})$  from other physics. We assume it is given by the nucleon value 4.7, with arbitrary error given by the full value 4.7. As we discussed in Section I C, there are a number of cases in the literature where the other matrix element contributing to  $b_M$  is not very large, and this range of  $b_M$  easily covers all the cases in the literature.

We list in Table I the fit results for  $A_T$  and  $d$  for different values of  $b_M$ , in hopes that further knowledge of  $b_M$  and  $d$  will eventually become available. We show the contributions to the fit from the different terms in Fig. 13.

$b_M/(AM_{GT})$	$d/A$	$A_T$	$\sqrt{\chi^2/N}$
9.4	$-34 \pm 42$	$0.034 \pm 0.032$	2.06
4.7	$-24 \pm 39$	$0.015 \pm 0.029$	1.90
0	$-14 \pm 36$	$-0.003 \pm 0.027$	1.76
-4.7	$-4 \pm 34$	$-0.022 \pm 0.025$	1.64
-9.4	$6 \pm 32$	$-0.040 \pm 0.024$	1.56
-14.1	$16 \pm 31$	$-0.059 \pm 0.023$	1.51
-18.8	$26 \pm 31$	$-0.078 \pm 0.023$	1.50
-23.5	$37 \pm 31$	$-0.096 \pm 0.024$	1.52
-18±11	$24 \pm 41$	$-0.074 \pm 0.050$	1.60

TABLE I: Results for fits to the dependence of the recoil asymmetry on recoil momentum for  $d/A$  and  $A_T$ , with  $N = 8$ .  $b_M/AM_{GT}$  is fixed at each of the values in the first column. We include the nucleon value of  $b_M/(AM_{GT}) = 4.7$ , and sweep through a large number of other values. The bottom line is the fit result if  $b_M$  is allowed to float unconstrained; note that this value for  $b_M$  is far outside the nucleon value.

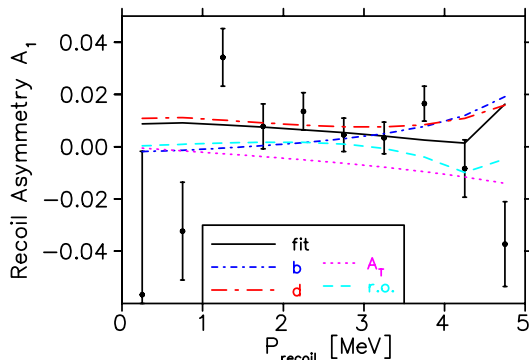


FIG. 13: (Color online) The dependence on recoil momentum of the recoil asymmetries for the best fit with  $C_T + C'_T=0$  (i.e. assuming the result of Ref. [7]), but  $b_M/(AM_{GT})=4.7\pm 4.7$ , with  $d$  and  $C_T - C'_T$  floating. The result is  $A_T=0.015\pm 0.029\pm 0.019$  (see text).

We interpret the results of this table to mean  $A_T=$

$0.015 \pm 0.029$  (statistical)  $\pm 0.001$  (systematic)  $\pm 0.019$  (theory syst). The first systematic error is from the nuclear polarization. The second systematic error is dominated by the error on  $b_M/(AM_{GT})$  of 100% of the nucleon value 4.7.

Then, by using Eq. 5, we can interpret our result for  $A_{\text{recoil}}$  to imply that  $C_T C'_T / C_A^2 = 0.012 \pm 0.022 \pm 0.015$ . We show the resulting 90% confidence limits in Fig. 10 as the green horizontal-hashed rectangular exclusion region showing  $|(C_T - C'_T)/C_A| \leq 0.36$  (with  $C_T + C'_T$  assumed 0). It can be seen that under these assumptions, we can place constraints on tensor interactions coupling to non-Standard Model right-handed neutrinos, i.e. on  $C_T - C'_T$ , competitive with constraints derived from the  $\beta$ - $\nu$  correlation in  ${}^6\text{He}$  [5, 6].

### D. Future improvements

In order to improve the precision of this experiment, 2nd-order recoil terms that might contribute to the  $1^+$  to  $2^+$  transition would have to be addressed. By adding efficient  $\gamma$ -ray detection to measure the recoils in coincidence with the 617 keV  $\gamma$  ray, the experimental asymmetry for the excited-state transition could be measured separately. Then it could be included in the model for the total asymmetry. That would allow the extraction of new physics from the  $1^+$  to  $0^+$  transition free of the complications of the higher-order recoil effects of the excited state transition. This would be necessary to improve the sensitivity to below the 0.01 level. Other improvements would include implementing the better optical pumping used in Ref. [23], which would improve accuracy by almost a factor of 2 by making the polarization close to 1.0.

An accurate simultaneous  $\beta$  asymmetry experiment as a function of  $\beta$  momentum could also help constrain the recoil-order terms.

Possible extensions of this experiment would include measuring the same quantity in  ${}^{82}\text{Rb}$  [31] as a nuclear structure consistency test in the same shell. The ground state transition is an 82% branch, and the lower Q-value (3.4 vs. 4.7 MeV) also would help reduce dependence on recoil-order terms. The  $3^+$  to  $2^+$  decay of the  ${}^{38}\text{K}$  ground state could also be used to search for tensor interactions—although several 2nd-order recoil nuclear matrix elements are needed, calculations in the SD shell could be done with reliable estimates of the theoretical error. Recoil asymmetry measurements in  ${}^8\text{Li}$  would require reconstruction of the momentum of the  $\alpha$  particles emitted, and could contribute to searches for 2nd-class tensor interactions [32] along with fundamental tensor interactions.

## V. CONCLUSIONS

We have used atom trap technology to make the first measurements of the asymmetry of daughter nuclei with respect to the nuclear spin, as suggested by Treiman [2]. By measuring the momentum dependence of the asymmetry, we can constrain the recoil order induced tensor  $d$  independently. The similar momentum dependence of weak magnetism  $b_M$  and the non-SM tensor physics  $b_T$  and  $A_T$  produces correlations in their extraction. So in Section IV above we have considered the constraints on non-SM tensor interactions from the present experiment, using different assumptions from other experiments and from theory.

If we make no assumption about tensor parameters from other experiments, and do not constrain  $b_M$  and  $d$ , then the 90% CL constraints are shown in Fig. 10. These are not competitive for tensors coupling to SM left-handed neutrinos, but their intersection with the vertical  $(C_T + C'_T) = 0$  axis shows the potential sensitivity of the technique.

We believe our most useful result is to assume that tensors coupling to SM left-handed neutrinos do not exist (i.e.  $C_T + C'_T = 0$ ) in accordance with Ref. [7], and let  $d$  float while constraining  $b_M/(AM_{GT})$  to the nucleon value with 100% error at one sigma. Then we extract  $A_T = 0.015 \pm 0.029$  (stat)  $\pm 0.019$  (syst). Eq. 5 then im-

plies  $C_T C'_T / C_A^2 = 0.012 \pm 0.022 \pm 0.015$ . The resulting constraints on tensor couplings to right-handed neutrinos  $|(C_T - C'_T)/C_A| < 0.36$  are also indicated in Fig. 10. These constraints are complementary to those from the  ${}^6\text{He}$   $\beta$ - $\nu$  correlation. We include Table I in hopes that future improvements in the knowledge of the recoil-order terms can be included.

So our results place constraints on tensor interactions complementary to those from other experiments. The systematic error is dominated by uncertainty in extracting recoil order corrections from our data, and there are no serious experimental systematics. The statistical error could be made considerably smaller with more counting and modest experimental improvements, which would cut the overall error by more than a factor of two even without theoretical guidance, and possibly by the order of magnitude that would make it complementary to the best measurements in nuclear, neutron, and pion decay.

## Acknowledgments

Supported by the Natural Sciences and Engineering Council of Canada, National Research Council Canada through TRIUMF, WestGrid, and the Israel Science Foundation.

- 
- [1] T.D. Lee and C.N. Yang, Phys. Rev. **104** 254 (1956)
- [2] S. B. Treiman, Phys. Rev. **110** 448 (1958); see Appendix A for correction of a typographical error in the equation for  $x_1$ .
- [3] J.D. Jackson, S.B. Treiman, and H.W. Wyld Jr., Nucl. Phys. **4** 206 (1957).
- [4] B.R. Holstein and S.B. Treiman, Phys. Rev. D **16** 2369 (1977); P. Herczeg, Phys. Rev. D **34** 3449 (1986).
- [5] C.H. Johnson, F. Pleasonton, and T.A. Carlson, Phys. Rev. **132** 1149 (1963)
- [6] F. Glück, Nucl. Phys. A **628** 493 (1998)
- [7] A.S. Carnoy, J. Deutsch, T.A. Girard, and R. Prieels, Phys. Rev. C **43** 2825 (1991)
- [8] N. Severijns, M. Beck, and O. Naviliat-Cuncic, Reviews of Modern Physics **78** 991 (2006)
- [9] P. Herczeg, Physical Review D **49** 247 (1994).
- [10] P.A. Quin, J. Deutsch, T.E. Pickering, J.E. Schewe, and P.A. Voytas, Physical Review D **47** 1247 (1993)
- [11] M. Skalsey, Physical Review C **49** R620 (1994).
- [12] A. Serebrov, V. Varlamov, A. Kharitonov, A. Fomin, Yu. Pokotilovski, P. Geltenbort, J. Butterworth, I. Krasnoschekova, M. Lasakov, R. Tal'daev, A. Vassiljev, O. Zherebtsov, Phys. Lett. B **605** 72 (2005).
- [13] Takeyasu M. Ito and Gary Prézeau, Phys. Rev. Lett. **94** 161802 (2005)
- [14] E. Frlež, D. Počanić, V.A. Baranov, W. Bertl, M. Bychkov, N.V. Khomutov, A.S. Korenchenko, S.M. Korenchenko, T. Kozłowski, N.P. Kravchuk, N.A. Kuchinsky, W. Li, R.C. Minehart, D. Mzhavia, B.G. Ritchie, S. Ritt, A.M. Rozhdestvensky, V.V. Sidorkin, L.C. Smith, I. Supek, Z. Tsamalaidze, B.A. VanDevender, E.P. Velicheva, Y. Wang, H.-P. Wirtz, and K.O.H. Ziock, Phys. Rev. Lett. **93** 181804 (2004)
- [15] M. Bychkov, D. Pocanic, B. A. VanDevender, V. A. Baranov, W. Bertl, Yu. M. Bystritsky, E. Frlez, V. A. Kalinikov, N. V. Khomutov, A. S. Korenchenko, S. M. Korenchenko, M. Korolija, T. Kozłowski, N. P. Kravchuk, N. A. Kuchinsky, W. Li, D. Mekterovic, D. Mzhavia, S. Ritt, P. Robmann, O. A. Rondon-Aramayo, A. M. Rozhdestvensky, T. Sakhelashvili, S. Scheu, U. Straumann, I. Supek, Z. Tsamalaidze, A. van der Schaaf, E. P. Velicheva, V. P. Volnykh, Y. Wang, and H.-P. Wirtz, arXiv:0804.1815.
- [16] A.A. Poblaguev, Phys. Rev. D **68** 054020 (2003).
- [17] P. Herczeg, Prog. in Part. and Nucl. Phys. **46/2**, 413 (2001).
- [18] S. Profumo, M.J. Ramsey-Musolf, and S. Tulin, Phys. Rev. D **75** 075017 (2007)
- [19] B. Holstein, Rev. Mod. Phys. **46** 789 (1984).
- [20] F.P. Calaprice, W. Chung, and B.H. Wildenthal, Phys. Rev. C **15** 2178 (1977).
- [21] T.B. Swanson, D. Asgeirsson, J.A. Behr, A. Gorelov, and D. Melconian, J. Opt. Soc. Am. B **15**, 2641 (1998).
- [22] A. Gorelov, D. Melconian, W.P. Alford, D. Ashery, G. Ball, J.A. Behr, P.G. Bricault, J.M.D'Auria, J. Deutsch, J. Dilling, M. Domsbysky, P. Dubé, J. Fingler, U. Giesen, F. Glück, S. Gu, O. Häusser, K.P. Jackson, B.K. Jennings, M.R. Pearson, T.J. Stocki, T.B. Swanson, and M. Trinczek, Phys. Rev. Lett. **94** 142501 (2005)
- [23] D. Melconian, J.A. Behr, D. Ashery, O. Aviv, P.G.

- Bricault, M. Dombisky, S. Fostner, A. Gorelov, S. Gu, V. Hanemaayer, K.P. Jackson, M.R. Pearson, I. Vollrath, Phys. Lett. B **649** 370 (2007).
- [24] E. L. Raab, M. Prentiss, Alex Cable, Steven Chu, and D. E. Pritchard, Phys. Rev. Lett. **59** 2631 (1987).
- [25] P.A. Vetter, J.R. Abo-Shaeer, S.J. Freedman, and R. Maruyama, Phys. Rev. C **77** 035502 (2008); N.D. Scielzo, S.J. Freedman, B.K. Fujikawa, I. Kominis, R. Maruyama, P.A. Vetter, and J.R. Viereg, Nucl.Phys.A **746** 677c (2004)
- [26] T.A. Carlson, W.E. Hunt, and M.O. Krause, Phys. Rev. **151** 41 (1966).
- [27] C. Thibault, F. Touchard, S. Büttgenbach, R. Klapisch, M. de Saint Simon, H. T. Duong, P. Jacquinet, P. Juncar, S. Liberman, P. Pillet, J. Pinard, J. L. Vialle, A. Pesnelle, and G. Huber, Phys. Rev. C **23**, 2720 (1981).
- [28] R.R. Goruganthu and W.G. Wilson, Rev. Sci. Instrum. **55** 2030 (1984); A. Müller, N. Djurić, G.H. Dunn, and D.S. Belić, Rev. Sci. Instrum. **57** 349 (1986).
- [29] T.A. Carlson, C.W. Nestor, Jr., T.C. Tucker, and F.B. Malik, Phys. Rev. **169** 27 (1968)
- [30] J.A. Behr, A. Gorelov, D. Melconian, M. Trinczek, W.P. Alford, D. Ashery, P.G. Bricault, L. Courneyea, J.M. D’Auria, J. Deutsch, J. Dilling, M. Dombisky, P. Dubé, F. Glück, S. Gryb, S. Gu, O. Häusser, K.P. Jackson, B. Lee, A. Mills, E. Paradis, M. Pearson, R. Pitcairn, E. Prime, D. Roberge, and T.B. Swanson, *et al.*, Eur. Phys. J. A direct (2005) DOI: 10.1140/epjad/i2005-06-097-9.
- [31] D. Feldbaum, H. Wang, J. Weinstein, D. Vieira, and X. Zhao, Phys. Rev. A **76** 051402(R) (2007).
- [32] D.H. Wilkinson Eur. Phys. J. A **7** 307 (2000).
- [33] O. Aviv, M.Sc. Thesis, Tel Aviv U., ‘Feasibility study of isospin mixing in  $^{36}\text{Ar}$  with a polarized mot’, 2004.

## APPENDIX A

We present here the analytic results for the recoil spin asymmetry as a function of recoil momentum, assuming no Fermi function. These are obtained from the expressions for the full angular distribution in Refs. [3] and [19] by integration over  $\nu$  and  $\beta$  momenta. See Ref. [33] for more details. The units set  $m_\beta=1$ .

The angular distribution of daughter nuclei with respect to the nuclear spin as a function of their momentum  $P_r$  is

$$\begin{aligned}
W[P_r, \theta]dP_r d(\cos \theta_r) &= [f_1(P_r) + b_T f_6(P_r) - (a_{\beta\nu} + \frac{cT}{3})f_2(P_r) + cT f_3(P_r) \\
&\quad - PA_T f_4(P_r)\cos(\theta_r) + cT f_5(P_r)\cos^2(\theta_r) \\
&\quad + Pb_T f_7(P_r)\cos(\theta_r)]dP_r d(\cos \theta_r).
\end{aligned}$$

Integration of these kinematic functions over recoil mo-

mentum  $P_r$  produces the terms in Eq. 1. We also include here the normalization effect of the Fierz interference term  $b_T$  and a similar effect  $b_T$  in the asymmetry term, each multiplied by  $m_\beta/E_\beta$  before integration over  $\beta$  energy. These terms are explicitly neglected in Eq. 1 and in Ref. [2].

Note that the effect of the normalization term scaling  $f_6$  is negligible in this work, because in Gamow-Teller decays  $A_{\text{recoil}}=0$  in the absence of tensor terms and the effects of  $f_6$  enter in higher order in the small tensor parameters. That is no longer true for mixed Fermi/Gamow-Teller transitions.

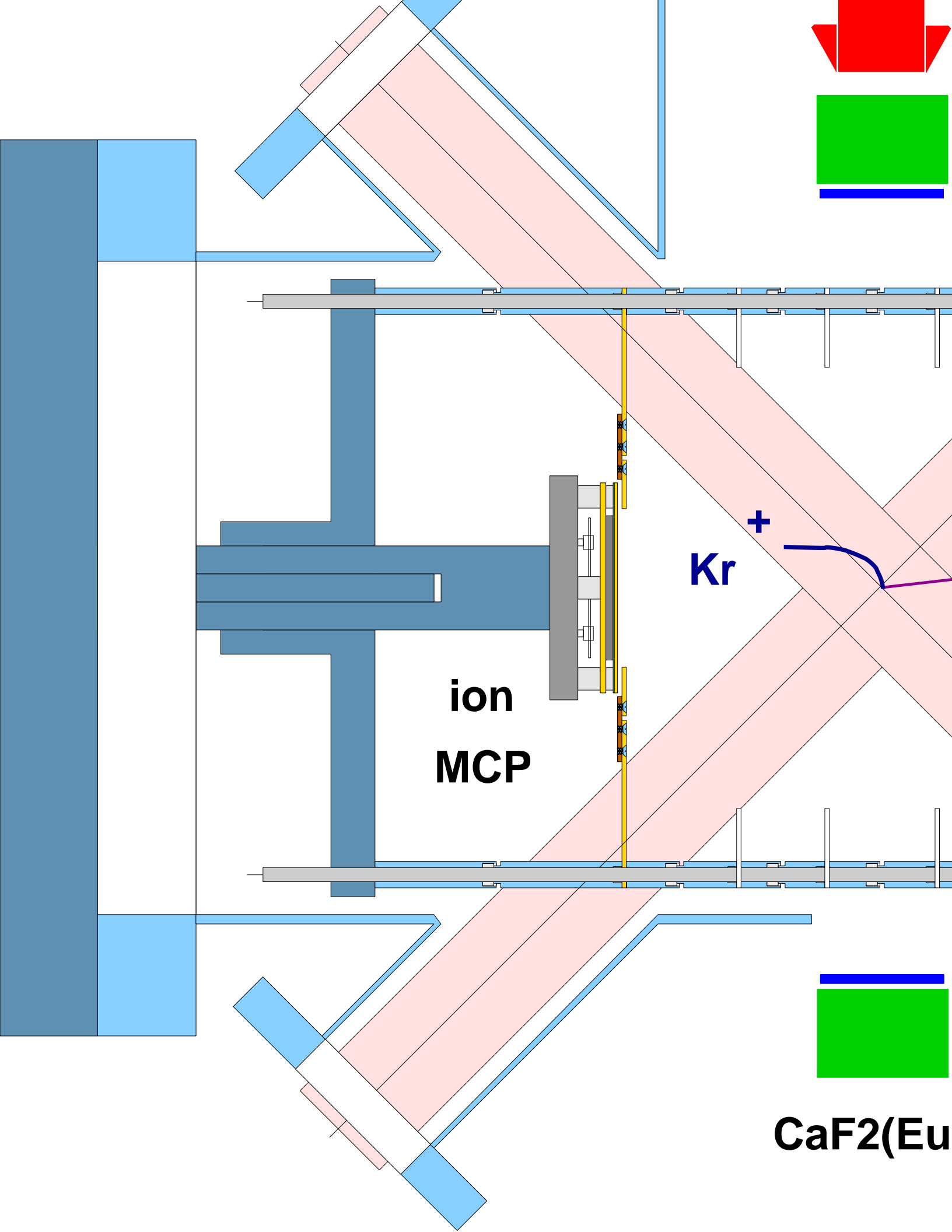
The kinematic functions of momentum are given by

$$\begin{aligned}
f_1(P_r) &= \frac{(P_r - E_0^2 P_r + P_r^3)^2 (3E_0^4 + P_r^2 + P_r^4 + E_0^2 (3 - 4P_r))}{12(E_0^2 - P_r^2)^3} \\
f_2(P_r) &= \frac{(P_r - E_0^2 P_r + P_r^3)^2 (3E_0^4 + P_r^2 (5P_r^2 - 1) - E_0^2 (3 + 8P_r^2))}{12(E_0^2 - P_r^2)^3} \\
f_3(P_r) &= -\frac{P_r^2 (1 - E_0^2 + P_r^2)^3}{12(E_0^2 - P_r^2)^2} \\
f_4(P_r) &= \frac{E_0 P_r^3 (2 + E_0^2 - P_r^2) (1 - E_0^2 + P_r^2)^2}{6(E_0^2 - P_r^2)^3} \\
f_5(P_r) &= -\frac{P_r^4 (2 + E_0^2 - P_r^2) (1 - E_0^2 + P_r^2)^2}{6(E_0^2 - P_r^2)^3} \\
f_6(P_r) &= \frac{E_0^3 P_r^2 - P_r^4 E_0 + 2E_0 P_r^2}{2(E_0^2 - P_r^2)} \\
f_7(P_r) &= \frac{(E_0^2 + P_r^2 + 1)(E_0^2 - P_r^2 - 1) - E_0^2 P_r (E_0^2 - P_r^2)}{2(E_0^2 - P_r^2)}
\end{aligned}$$

where  $E_0$  is the maximum total energy of the  $\beta$ , and where energies and momenta are in units of  $m_\beta$ . Integrating over the daughter nucleus momentum produces the terms needed in Eq. 1:

$$\begin{aligned}
x_1 &= \frac{5(E_0^5 - 6E_0^3 + 3E_0 + \frac{2}{E_0}) + 12E_0 \ln E_0}{4\sqrt{E_0^2 - 1}(2E_0^4 - 9E_0^2 - 8) + A_{ln}} \\
x_2 &= \frac{\sqrt{E_0^2 - 1}(4E_0^4 - 28E_0^2 - 81) + 15(6 + \frac{1}{E_0})A}{4\sqrt{E_0^2 - 1}(2E_0^4 - 9E_0^2 - 8) + A_{ln}} \\
A_{ln} &= \ln(E_0 + \sqrt{E_0^2 - 1})
\end{aligned}$$

Note the typographical error in the equation for  $x_1$  in Ref. [2].



**ion  
MCP**

**Kr<sup>+</sup>**

**CaF<sub>2</sub>(Eu)**